Noname manuscript No.
(will be inserted by the editor)

Dynamical behavior and network analysis of an extended Hindmarsh-Rose neuron model

Karthikeyan Rajagopal · Abdul Jalil M. Khalaf · Fatemeh Parastesh · Irene Moroz · Anitha Karthikeyan · Sajad Jafari

Received: date / Accepted: date

Abstract In this paper, the extended Hindmarsh-Rose neuron model, which considers the slow intracellular exchange of calcium ions between its store and the cytoplasm, is studied. The dynamical behavior of this neuron model is analyzed by deriving the equilibrium points, the bifurcation diagrams, and the Lyapunov exponents, in the presence of an external forcing current. Furthermore, the dynamics of the network of the extended model is investigated. Firstly, a one-dimensional ring network is constructed, and the effects of the coupling strength and the forcing current are considered on the network behavior. The results confirm the existence of chimera state in small coupling strength values. Then a square network of the proposed model is created by adding an external excitation to the neurons and four cases of different parameters are considered. Particularly, the effects of the stimulus parameters, the external current, and the coupling strength are studied on the emergence of spiral waves.

Keywords Extended Hindmarsh-Rose neuron model · bifurcation analysis · Chimera state · Spiral wave

K. Rajagopal · A. Karthikeyan
Center for Nonlinear Dynamics, Institute of Research and Development, Defence University, Ethiopia.

K. Rajagopal
Institute of Energy, Mekelle University, Ethiopia.

A. J. M. Khalaf
Ministry of Higher Education and Scientific Research, Baghdad, Iraq.

F. Parastesh
Department of Biomedical Engineering, Amirkabir University of Technology, Tehran, Iran.

I. Moroz
Mathematical Institute, University of Oxford, Andrew Wiles Building, Oxford, UK.

S. Jafari
Nonlinear Systems and Applications, Faculty of Electrical and Electronics Engineering, Ton Duc Thang University, Ho Chi Minh City, Vietnam.
E-mail: sajadjafari83@gmail.com

1 Introduction

The nervous system is made up of billions of smaller building blocks called neurons. These neurons are the main components of information transferring process which interact with each other [1]. The dynamical behavior of the neurons has attracted many researchers in recent years because of their role in transmitting the brain impulses and signal measurements [2]. The mathematical modeling of the neurons behavior is a challenging subject due to the complexities of the involved parameters. The Hindmarsh-Rose (HR) model [3,4] can describe the bursting and spiking phenomenon of the neurons which are of significance in studying the dynamics of neurons. Since the presence of HR model, there have been many works in the literature, focusing on the study of the dynamics of the original HR model and also the effects of various external forces on the HR model [5–8].
Various neurological studies show the relevance of the dynamical behaviors of the neurons and the resting potentials. Hence neurons may exhibit chaotic oscillations during the bursting and spiking modes [9,10]. Mainly such chaotic oscillations occur during the transition between the bursting and spiking phases, which participate in information transferring process [9]. The transmission of the encoded information generally depends on the capability of the neurons in synchronizing with

their neighbors [11]. Electrical and chemical synapses have an important role in information transmission between neurons and are often used to investigate the synchronization. However, signal exchanging can also occur by flow of ion currents in the case of field coupling [12]. Recently, the effect of electromagnetic field has been investigated on the collective behavior of neurons [13–15]. Thus the analysis of synchronization of neuronal networks is an important research area and has attracted considerable attention [16–21]. These studies are often considered as efficient mechanisms in identifying neural disorders such as Parkinson [22].

Many biological systems show collective behaviors such as chimera state and wave propagation which are observed in real-world situations [23, 24]. The chimera state is denoted by the coexistence of coherent and incoherent groups in the network of identical oscillators [25–28]. The chimera state has strong relevance with some real phenomena including neuronal diseases [29]. Thus it has been studied extensively in neuronal networks [29–32]. On the other hand, the wave propagation plays an important role in the excitable biological cells [33]. Spiral wave is a special self-organized pattern which seems to be a considerable fundamental of reentrant excitation in the cardiac tissue [34]. Therefore, the study of spiral waves has achieved significant attention in recent years [34–36].

Motivated by the above literature, in this paper, an extended version of the HR model is analyzed, wherein the slow intracellular exchange of calcium ions between its store[37, 38] and the cytoplasm is considered [39]. In section two the mathematical model of the extended HR model is given. In section three the complete dynamical properties of the HR model such as equilibrium points, stability analysis, Lyapunov spectrum, and bifurcations are studied. Section four and five present the network analysis of the proposed model and discuss the emergence of chimera state and spiral wave. Finally, the conclusions are presented in section six.

2 Extended Hindmarsh-Rose neuron model (EHRN)

The simplest model for neuron [4] has been proposed by two differential equations as:

$$\begin{aligned} \dot{x} &= a(y - f(x)) + u \\ \dot{y} &= b(g(x) - y) \end{aligned} \tag{1}$$

where x represents the membrane potential and y represents the recovery variable, with $f(x)$ and $g(x)$ representing the cubic and quadratic nonlinear function. Considering the effects of spiking and also the fact that the firing frequency of the cell is not uniform and can slow down and vanishes, Eq. (1) was modified by including a third state which represents the hyperpolarizing current [3]. The resulting equation is known as the Hindmarsh-Rose neuron model given as:

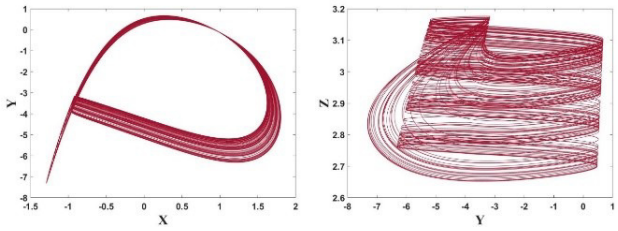

Fig. 1 2D phase portraits of the EHRN model Eq. (3) for $I_{ext} = 3$.

$$\begin{aligned} \dot{x} &= y - ax^3 + bx^2 - z + I_{ext} \\ \dot{y} &= c - 5x^2 - y \\ \dot{z} &= r(s(x + 1.56) - z) \end{aligned} \tag{2}$$

where the variables x, y, z describe the membrane potential, slow current for recovery variable and adapting current, respectively, with I_{ext} denoting the external forcing current. However, the model of Eq. (2) cannot represent the exact behavioral pattern of the neurons due to its complex nonlinearity. To solve this, a fourth dimension was added to Eq. (2), which describes the slow intracellular exchange of calcium ions between its store and the cytoplasm [39, 40]. The resulting four-dimensional neuron model was named as the extended HR model (EHRN) and is expressed as:

$$\begin{aligned} \dot{x} &= y - ax^3 + bx^2 - z + I_{ext} \\ \dot{y} &= c - 5x^2 - y - (1/80)w \\ \dot{z} &= r(s(x + 1.56) - z) \\ \dot{w} &= d(-w + e(y + 0.9)) \end{aligned} \tag{3}$$

where a, b, c, d, e, r, s are the system parameters, the values of which are defined as:

$$\begin{aligned} &a = 1, b = 3, c = 1, d = 0.0002, r = 0.006, s = 4, \\ &e = 0.88 \end{aligned} \tag{4}$$

The external excitation current I_{ext} is considered as the control parameter of the system Eq. (3) and the paper focuses on the dynamical analysis of the EHRN for various values of the current I_{ext}. Figure 1 shows the 2D phase portraits of the EHRN model for $I_{ext} = 3$.

3 Dynamical analysis of EHRN

The dynamical properties of the EHRN system such as equilibrium points, eigenvalues, Lyapunov spectrum, and bifurcation plots are derived and discussed in this section.

3.1 Equilibrium points and stability analysis

The fixed points of Eq. (3) are obtained by setting the time derivatives of Eq. (3) to zero as calculated in [37]. For the parameter set given in Eq. (4), the equation for obtaining the fixed points becomes as:

$$x_e^3 + 1.9456x_e^2 + 4x_e + 5.26067 - I_{ext} = 0 \tag{5}$$

Numerical calculations show that for $-10 \leq I_{ext} \leq 10$ there is one real root to Eq. (5), which increases monotonically between $-2.63046 \leq I_{ext} \leq 0.7756$ and a pair of complex conjugate roots, whose imaginary parts do not vanish. Figure 2a shows the real-valued fixed points for $0 \leq I_{ext} \leq 10$.

The linear stability of the real fixed point is determined from the fourth order Jacobian matrix [37], and the associated characteristic equation:

$$\lambda^4 + B_3\lambda^3 + B_2\lambda^2 + B_1\lambda + B_0 = 0 \tag{6}$$

where:

$$\begin{aligned}
B_3 &= r + d + 1 + 3ax_e^2 - 2bx_e \\
B_2 &= r + d + rd + de/80 + (3ax_e^2 - 2bx_e)(r + d + 1) \\
&\quad + 10x_e + rs \\
B_1 &= rd(1 + e/80) + (3ax_e^2 - 2bx_e)(r + d + rd + de/80) \\
&\quad + 10x_e(r + d) + rs(1 + d) \\
B_0 &= rd(1 + e/80)(3ax_e^2 - 2bx_e) + rd(10x_e + s(1 + e/80))
\end{aligned} \tag{7}$$

The choice of parameter values leads to the coefficient B_0 varying between the order of 10^{-6} and 10^{-5}. Figure 2b shows the linear stability curves in a region of the zero-eigenvalue line. As I_{ext} varies in the range $0 \leq I_{ext} \leq 10$, there are always two real eigenvalues. One eigenvalue is real, initially large and negative, while another eigenvalue is of order 10^{-4}, and remains very small throughout. For $0 \leq I_{ext} \leq 1.12$, there is a pair of complex conjugate eigenvalues with a negative real part. A Hopf bifurcation occurs at $I_{ext} \approx 1.13$. When $I_{ext} \approx 2.14$, there are four real eigenvalues, two of which are positive. Therefore, there is a saddle-node bifurcation. All four eigenvalues remain real until $I_{ext} \approx 4.81$, when a second saddle-node bifurcation occurs, and again there is a pair of complex conjugate eigenvalues with positive real parts. This pair crosses the imaginary axis when $I_{ext} \approx 5.26$; the real parts remain negative, until $I_{ext} \approx 6.04$, when a third Hopf bifurcation occurs. Thereafter the complex eigenvalues have positive real parts.

Criteria for a Hopf bifurcation can be identified by substituting $\lambda = i\omega$ into the characteristic equation. Equating real and imaginary parts leads to the condition that ω^2 must be a common positive root of $\omega^4 - B_2\omega^2 + B_0 = 0$ and quadratic $\omega^2 = B_1/B_3$. Eliminating ω^2 between these two equations yields the equation Eq. (8) for the Hopf bifurcation curve,

$$B_1^2 - B_1B_2B_3 + B_0B_3^2 = 0 \tag{8}$$

It is remarked that due to the existence of a Hopf bifurcation at $I_{ext} \approx 2.13$, the remaining bifurcations are not observed in the nonlinear integrations. The appearance of a stable periodic limit cycle, and its subsequent transitions to chaotic dynamics, cover the range of I_{ext} at which the linear stability analysis predicts interesting bifurcations.

3.2 Bifurcation analysis and Lyapunov spectrum

The dynamical behavior of the EHRN model can be understood by studying the bifurcation plots of the model. For deriving the bifurcation diagrams, the external excitation current I_{ext} is considered as the control parameter and the local maxima of the state x is plotted. Figure 3a shows the bifurcation of the EHRN model at which several regions of periodic oscillations and period doubling route to chaos is observed. For the region $1.5 \leq I_{ext} \leq 1.9$, period-2 oscillations are observed, as shown in Fig. 3a as 'P-2' and for $1.9 \leq I_{ext} \leq 2.4$, a period-3 oscillation is observed, denoted by 'P-3' in Fig. 3a. Similarly, a period-4 oscillation region can be observed for $2.4 \leq I_{ext} \leq 2.7$ and each period in 'P-4' undergoes period doubling route to chaos for the region $2.7 \leq I_{ext} \leq 3.25$. The corresponding Lyapunov exponents (LEs) are calculated using the Wolf algorithm [7] for a fixed time of $40000s$, and are shown in Fig. 3b.

Indeed the onset of a Hopf bifurcation was verified with integrating the nonlinear four-dimensional system, by both increasing and decreasing I_{ext}. The results are shown in Fig. 3c. Note the hysteresis at the boundaries of transition between different periods.

4 Chimera state in 1D Network of the EHRN

To further capture the complex dynamics of the EHRN, a ring network of neurons is constructed. Therefore,

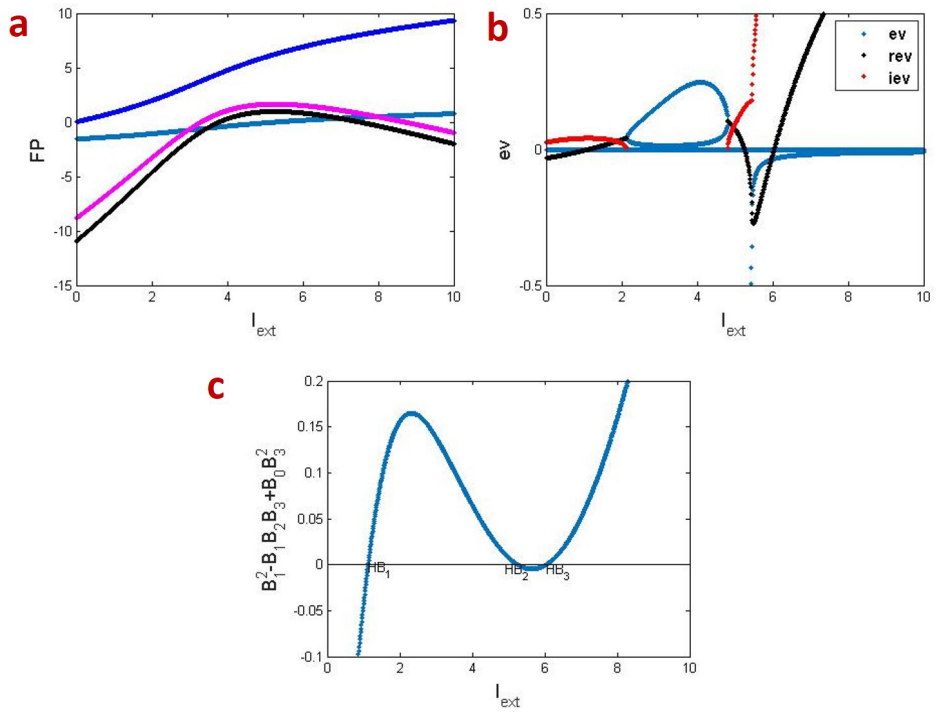

Fig. 2 a) The locus of fixed points for the neuron Eq. (3) as I_{ext} varies. The pale blue line corresponds to x, the black line to y, the darker blue line to z and the magenta line to w. b) Eigenvalues for the linear stability of the fixed point x_e as I_{ext} varies. The blue curve corresponds to the real eigenvalues, while the black and red curves correspond to the real and imaginary parts of the complex conjugate pair of eigenvalues. c) Hopf bifurcation condition shown by Eq.(8), where the curve crosses the x axis is the location of the HB points. It can be seen that HB_1 is at $I_{ext} = 1.131$; HB_2 is at $I_{ext} = 5.26$ and HB_3 is at $I_{ext} = 6.04$.

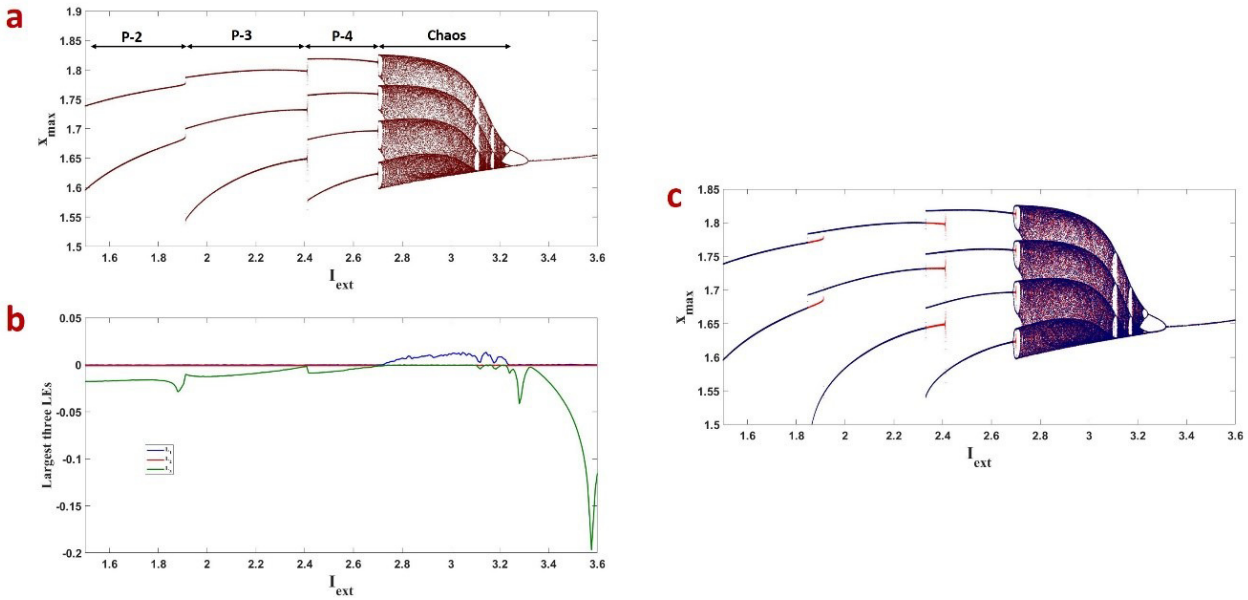

Fig. 3 a) Bifurcation, b) Lyapunov spectrum and c) The bifurcation transition plots as I_{ext} increases (blue) and decreases (red).

the neurons are coupled non-locally to the nearby $2M$ neighbors with a coupling strength of D. The ring network structure of the neurons can be defined as:

$$\begin{aligned}\dot{x}_i &= y_i - ax_i^3 + bx_i^2 - z_i + I_{ext} + \tfrac{D}{2M}\sum_{j=i-M}^{i+M}(x_j - x_i)\\ \dot{y}_i &= c - 5x_i^2 - y_i - (1/80)w_i\\ \dot{z}_i &= r(s(x_i + 1.56) - z_i)\\ \dot{w}_i &= d(-w_i + e(y_i + 0.9))\end{aligned} \tag{9}$$

where $i = 1, ..., N$ and N is the total number of nodes. In order to derive the dynamics of the neuronal ring network, the parameters are fixed as given in Eq. (4) and $N = 100$, $M = 25$. In the simulations, the network is investigated by varying the excitation current I_{ext} or the coupling strength D. Thus, the discussions can be divided into two different cases as:

Case-A: For fixed I_{ext} and by varying D.

Case-B: For fixed D and by varying I_{ext}.

Figure 4 shows the spatiotemporal patterns of the ring neuronal network for case-A where the external excitation current is fixed as $I_{ext} = 3$ and the coupling strength is varied. It can be seen that for a coupling strength close to zero, the system doesn't have any synchronization and the neurons are asynchronous. By increasing the coupling strength to 0.1, it is observed that the system exhibits the chimera state. For the coupling strength values more than 0.5, the system moves toward synchronization, and hence the chimera state disappears.

For the second case, the spatiotemporal patterns are considered for fixed coupling strength and varying I_{ext}. The results are shown in Fig. 5. At first, the coupling strength is fixed at $D = 0.01$ (the top row of Fig. 5). In this case, the network is in the asynchronous state until the external current reaches to $I_{ext} = 3.5$, at which some small coherent groups are formed in the network. Then the coupling strength is increased to $D = 0.25$ (the middle row of Fig. 5). In this case, the bursting states of the neurons are composed of both synchronous and asynchronous groups leading to chimera state. Varying the external current changes the number of neurons in the coherent and incoherent groups. By Further increasing of the coupling strength to $D = 0.5$, one can observe that the chimera state disappears and the system enters the synchronous regime.

5 Spiral waves in 2D network of externally excited EHRN model

To computationally analyze the formation of spiral wave in the EHRN, we construct the coupled neuronal network of size 110×110. An external stimulation $\xi(t) = A cos(\omega t)$ is applied to the neuronal network for triggering the wave formation, where A, ω represent the stimulus amplitude and frequency, respectively. The coupling strength between the neurons of the network is D and the stimulation excitation is present for the entire period of simulation. The parameters used for the discussion on the birth and death of spiral waves, are the excitation current I_{ext}, the parameters of the external periodical force A, ω, and the coupling strength D. The 4^{th} order Runge-Kutta is used for numerical calculation of the network with no-flux boundary condition, and with time step $h = 0.001$. The initial states of the variables are $(x, y, z, w) = [0.01, 0.02, 0.003, 1.01]$ and the simulation period is about $15000-$time units. The spatiotemporal patterns of the membrane potential are observed and the snapshots of the resulting patterns are displayed in $t = 15000-$time units. In the snapshots, the level of excitability of the neurons is represented by the color. The EHRN network of 110×110 can be defined as,

$$\begin{aligned}\dot{x}_{ij} &= y_{ij} - ax_{ij}^3 + bx_{ij}^2 - z_{ij} + I_{ext} + D(x_{i+1,j} + x_{i-1,j}\\ &+x_{i,j-1} + x_{i,j+1} - 4x_{i,j}) + \xi(t)\phi_{i,\theta_1}\phi_{j,\theta_2}\\ \dot{y}_{ij} &= c - 5x_{ij}^2 - y_{ij} - (1/80)w_{ij}\\ \dot{z}_{ij} &= r(s(x_{ij} + 1.56) - z_{ij})\\ \dot{w}_{ij} &= (-w_{ij} + e(y_{ij} + 0.9))\end{aligned} \tag{10}$$

where $\xi(t) = A cos(\omega t)$ is the stimulus, and

$$\begin{cases}\phi_{i\theta_1} = 1, \text{ for } i = \theta_1\\ 0, \text{ otherwise}\end{cases}, \quad \begin{cases}\phi_{j\theta_2} = 1, \text{ for } j = \theta_2\\ 0, \text{ otherwise}\end{cases} \tag{11}$$

The stimulus $\xi(t)$ is imposed on the left boundary by setting $\theta_1 = 2 : 108$ and $\theta_2 = 1$. We discuss the generation of spiral waves under four different cases as

Case-1: Fixed stimulus amplitude, frequency and coupling strength D, and varying I_{ext}.

Case-2: Fixed stimulus amplitude, coupling strength D and I_{ext}, and varying stimulus frequency.

Case-3: Fixed stimulus amplitude, frequency and I_{ext}, and varying coupling strength D.

Case-4: Fixed stimulus frequency, $I_e xt$ and coupling strength D, and varying stimulus amplitude.

5.1 Spiral waves in case-1

In the first case, the generation of spiral waves is discussed for fixed stimulus amplitude, stimulus frequency, coupling strength (D) and varying the external excitation current. The snapshots of the membrane potential, at time $t = 15000s$, are shown in Fig. 6. Firstly,

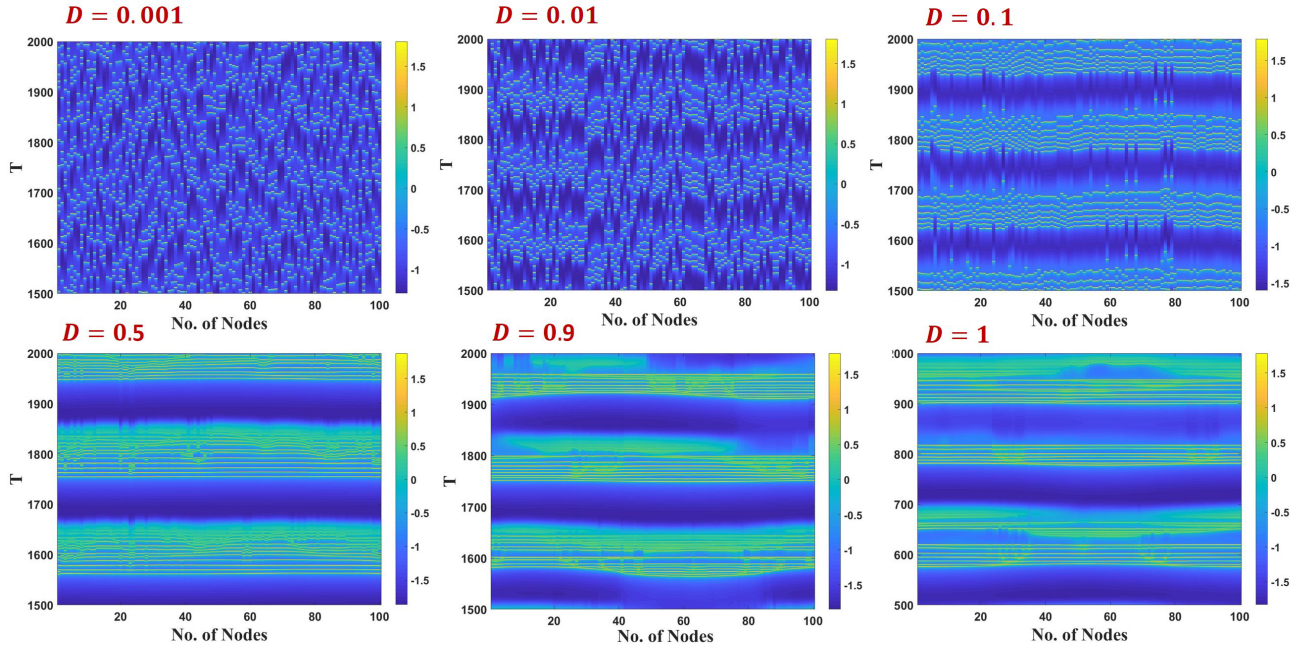

Fig. 4 Spatiotemporal patterns of the ring neuronal network for fixed $I_{ext} = 3$ and different coupling strength values.

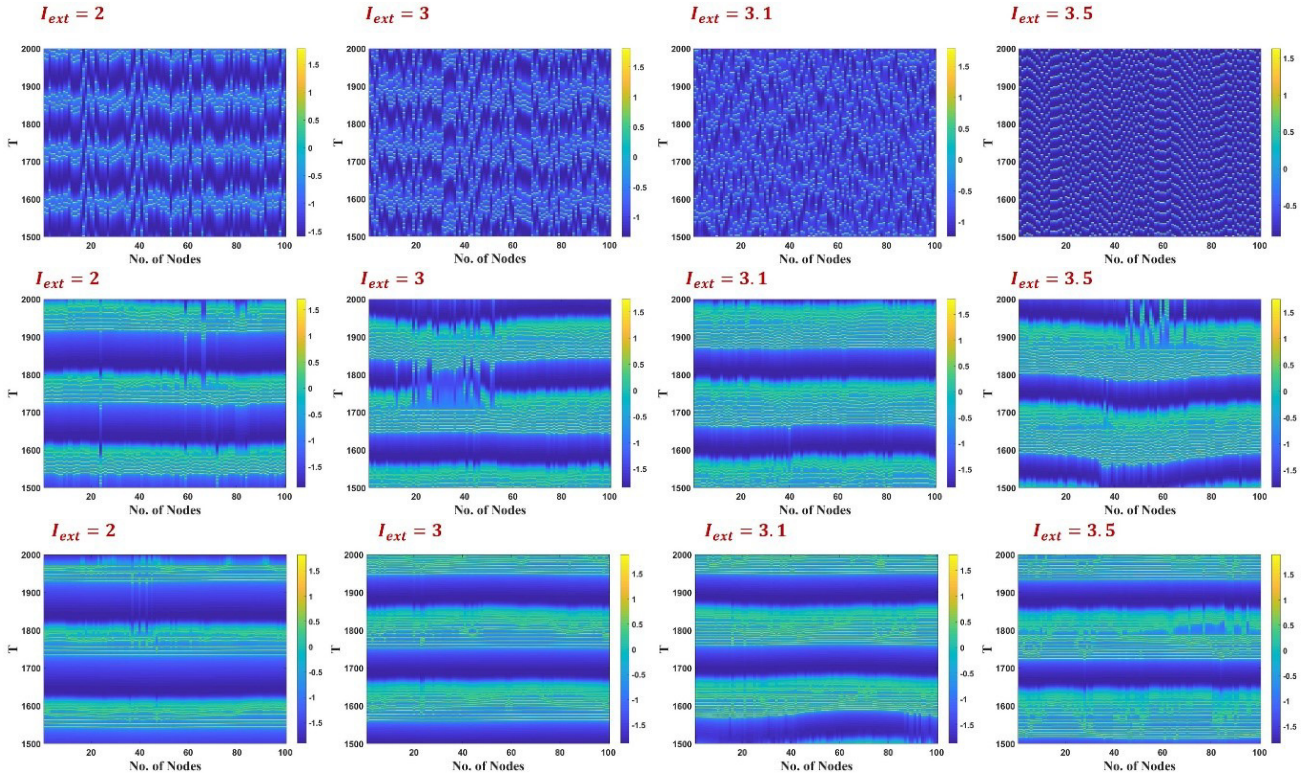

Fig. 5 Spatiotemporal patterns of the ring neuronal network for different values of I_{ext} and fixed coupling strength of $D = 0.01$ (top row), $D = 0.25$ (middle row) and $D = 0.5$ (bottom row).

the value of $I_{ext} = 2.9$ is considered and it can be verified from Fig. 3a that the system is in chaos region for this I_{ext} value. The stimulus amplitude and frequency are fixed at $A = 2$ and $\omega = 0.0001$, with $D = 1$. Figure 4 indicates that there is no sign of a spiral seed or spiral circuit in the snapshot. The result is similar for $I_{ext} = 2.95$, with no spiral wave formation. But when the external excitation current is increased to $I_{ext} = 3$, one can see the birth of spiral waves with a singular spiral seed. This spiral seed breaks into two spiral seeds when the excitation current is further increased to $I_{ext} = 3.1$. These cases of $I_{ext} = 3$ and $I_{ext} = 3.1$ are considered to be special cases of the EHRN model. Further increasing of I_{ext} makes the plane waves stronger and destroys the spiral seeds.

5.2 Spiral waves in case-2

In the second case, the stimulus frequency ω is varied, while keeping the stimulus amplitude fixed at $A = 2$, the external excitation current at $I_{ext} = 3$ and the coupling strength at $D = 1$. Figure 7 shows the snapshots of the membrane potential captured at 15000−time units. It is observed that for a very low stimulus frequency of $\omega = 0.00001$, there is no spiral seed. Increasing the frequency to $\omega = 0.0001$, clearly indicates a spiral seed with multiple orbits centered around that. Further increasing of frequency to $\omega = 0.001$, the spiral seed splits into two spiral orbits. Finally, an increase in frequency to $\omega = 0.01$, leads to the power of plane waves and the annihilation of spiral seeds.

5.3 Spiral waves in case-3

The third case is to discuss the impact of the coupling strength on the generation of spiral waves. Therefore, the coupling strength D is considered as the control parameter and the stimulus amplitude, frequency and excitation current are taken as $2, 0.0001$ and 3, respectively. The resulting snapshots of the membrane potentials are shown in Fig. 8. When the coupling strength takes the values of 0.91 and 0.92, there is no evidence of spiral waves in the network. Whereas when the coupling strength is increased to 0.93, two spiral seeds are seen which further grow to spiral orbits. More increasing of coupling strength destroys the spiral seeds such that the spiral waves are not formed for $D = 0.95$ and $D = 0.98$ and $D = 0.99$, as shown in Fig. 8. But when the coupling strength reaches to $D = 1$, again the spiral waves appear in the network.

5.4 Spiral waves in case-4

In the final discussion, the effect of the stimulus amplitude on the generation of spiral waves is investigated. The stimulus frequency, excitation current, and the coupling strength are taken as 0.0001 and 3 and 1, respectively. Figure 9 shows the snapshots of the membrane potentials in this case. For the amplitude $A = 1$, there are no spiral seeds in the network. When the stimulus amplitude is increased to $A = 2$, the spiral waves are formed, while for $A = 3$ the spiral seed is dissipated.

6 Conclusion

In this paper, we studied the dynamics of the extended Hindmarsh-Rose neuron model with the forth variable describing the slow intracellular exchange of calcium ions. At first, complete dynamical behavior of the extended HR model was analyzed. The equilibrium points and their stability, the bifurcation diagrams and the Lyapunov exponents were derived and discussed. The existence of chaos and the effect of an external forcing current on the chaotic oscillations were also studied. In addition, due to the influence of the elements' dynamics on the collective behaviors in the networks, the network of the extended model was investigated. The synchronization dynamics of the EHRN model was captured by constructing a ring network of neurons. It was observed that the chimera state is emerged in lower coupling strength values and increasing the coupling strength leads to the synchronization of the neurons. Finally, a two-dimensional network was constructed with considering an external stimulation. The birth and death of spiral waves were studied under different parameters' sets. It was found that the formation of the spiral waves is achieved in specific ranges of stimulus parameters and the external current. The parameter values lower than the defined range, cannot form the spiral seeds and the higher values make the plane waves stronger and destroy the spiral seeds.

For future studies we recommend analyzing the EHRN system in the presence of the external magnetic excitation and electromagnetic induction. Also one can consider a periodic forcing current instead of the constant one.

Conflict of interest

The authors declare no conflict of interests.

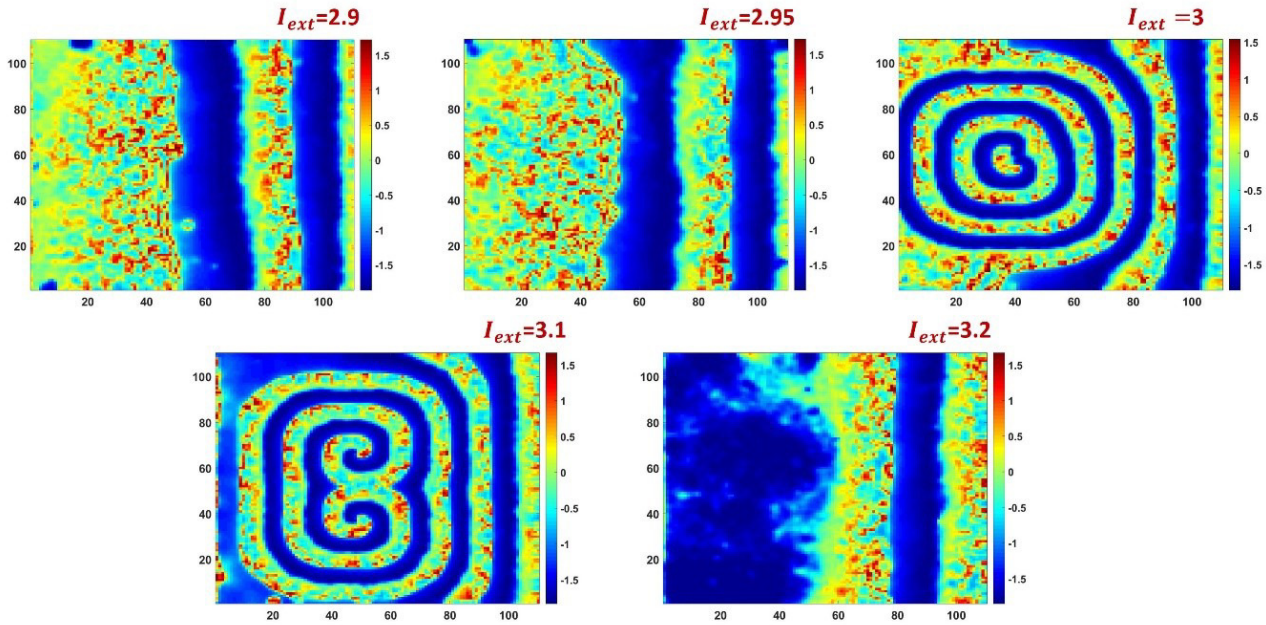

Fig. 6 The time-snapshots of the neurons' membrane potential for various values of I_{ext} in case-1.

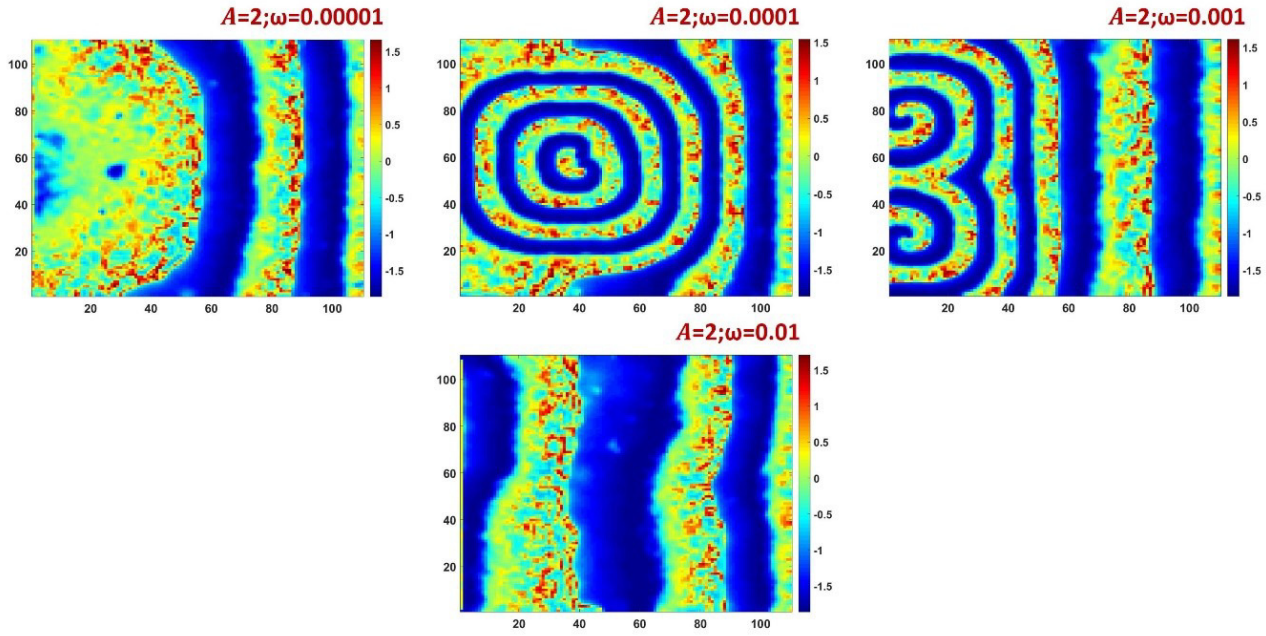

Fig. 7 The time-snapshots of the neurons' membrane potential for various values of the stimulus frequency in case-2.

References

1. J. Ma, J. Tang, A review for dynamics of collective behaviors of network of neurons, Sci. China Technol. Sci. 58 (12) (2015) 2038–2045.
2. J. Ma, J. Tang, A review for dynamics in neuron and neuronal network, Nonlinear Dynam. 89 (3) (2017) 1569–1578.
3. J. L. Hindmarsh, R. Rose, A model of neuronal bursting using three coupled first order differential equations, Proc. R. Soc. Lond. B 221 (1222) (1984) 87–102.
4. G. Houart, G. Dupont, A. Goldbeter, Bursting, chaos and birhythmicity originating from self-modulation of the inositol 1, 4, 5-trisphosphate signal in a model for intracellular ca2+ oscillations, Bull. Math. Biol. 61 (3) (1999) 507–530.
5. D. Jun, Z. Guang-jun, X. Yong, Y. Hong, W. Jue, Dynamic behavior analysis of fractional-order hindmarsh–rose neuronal model, Cogn. Neurodynam. 8 (2) (2014) 167–175.
6. S. Lakshmanan, C. P. Lim, S. Nahavandi, M. Prakash, P. Balasubramaniam, Dynamical analysis of the

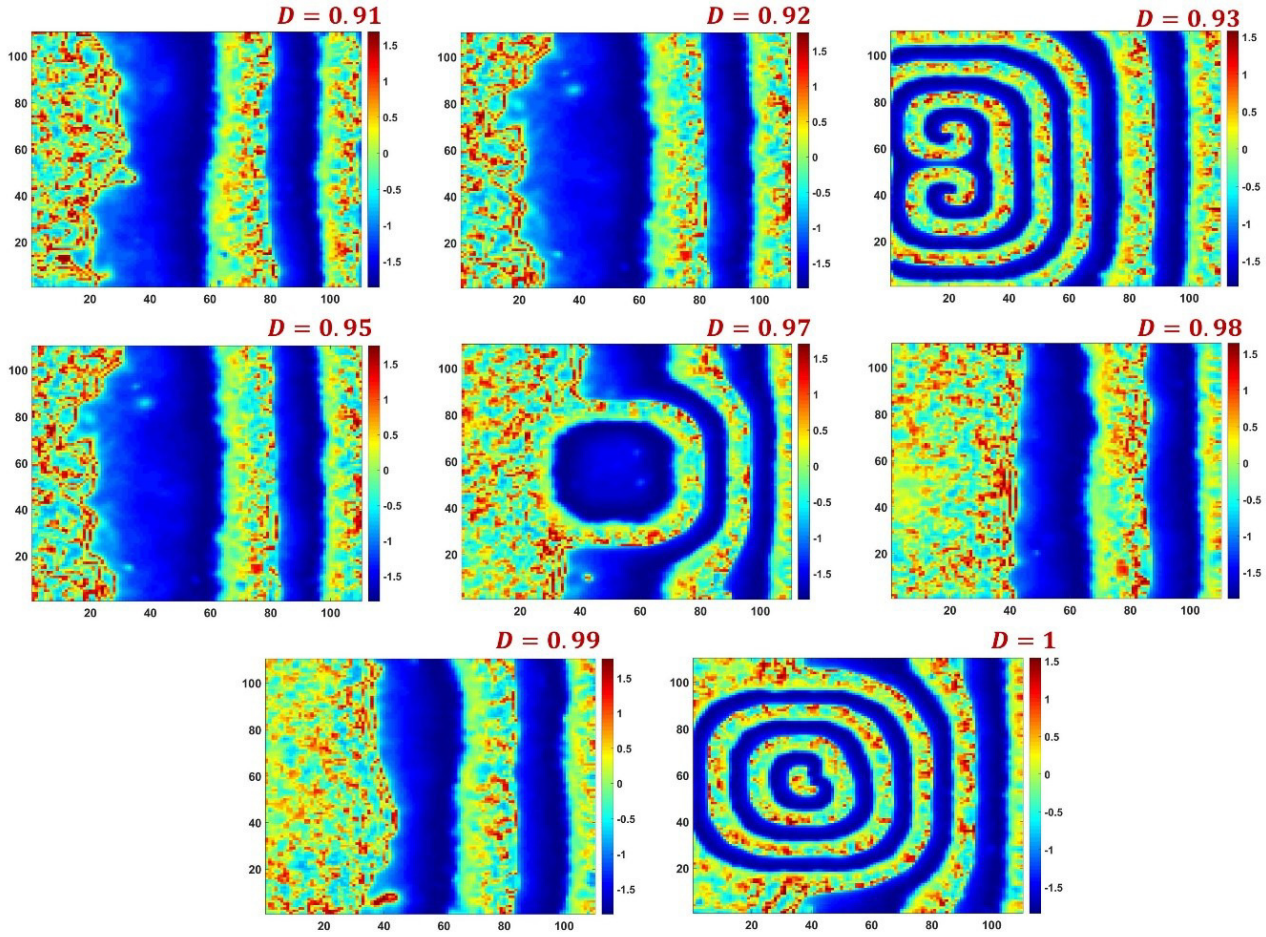

Fig. 8 The time-snapshots of the neurons' membrane potential for various values of the coupling strength in case-3.

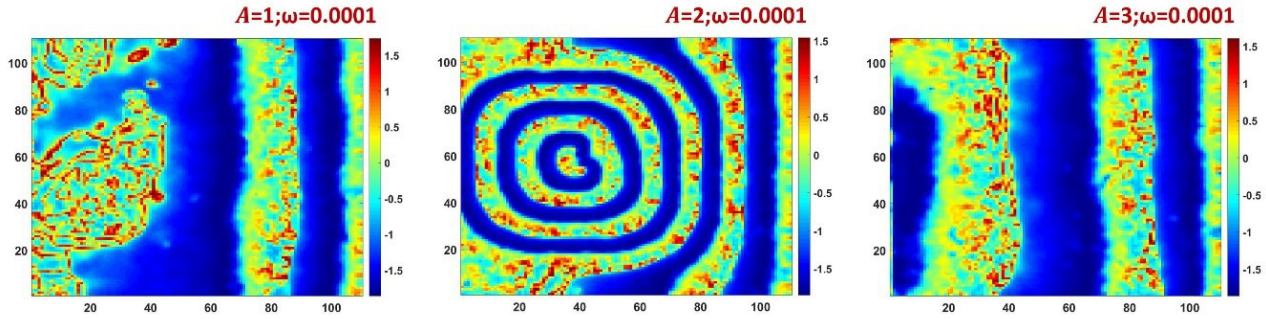

Fig. 9 The time-snapshots of the neurons' membrane potential for various values of the stimulus amplitude in case-4.

hindmarsh–rose neuron with time delays, IEEE Trans. Neural Networks Learn. Syst. 28 (8) (2017) 1953–1958.
7. M. Lv, J. Ma, Multiple modes of electrical activities in a new neuron model under electromagnetic radiation, Neurocomputing 205 (2016) 375–381.
8. S. Panahi, S. Jafari, A. J. M. Khalaf, K. Rajagopal, V.-T. Pham, F. E. Alsaadi, Complete dynamical analysis of a neuron under magnetic flow effect, Chin. J. Phys. 56 (5) (2018) 2254–2264.
9. S. Dtchetgnia Djeundam, R. Yamapi, T. Kofane, M. Aziz-Alaoui, Deterministic and stochastic bifurcations in the hindmarsh-rose neuronal model, Chaos 23 (3) (2013) 033125.
10. F. Parastesh, K. Rajagopal, F. E. Alsaadi, T. Hayat, V.-T. Pham, I. Hussain, Birth and death of spiral waves in a network of hindmarsh–rose neurons with exponential magnetic flux and excitable media, Appl. Math. Comput. 354 (2019) 377–384.
11. W. Qing-Yun, L. Qi-Shao, Time delay-enhanced synchronization and regularization in two coupled chaotic neurons, Chin. Phys. Lett. 22 (3) (2005) 543.
12. S. Guo, Y. Xu, C. Wang, W. Jin, A. Hobiny, J. Ma, Collective response, synapse coupling and field coupling in neuronal network, Chaos, Solitons & Fractals 105 (2017)

120–127.
13. M. Lv, J. Ma, Y. Yao, F. Alzahrani, Synchronization and wave propagation in neuronal network under field coupling, Sci. China Technol. Sci. 62 (3) (2019) 448–457.
14. Y. Xu, Y. Jia, J. Ma, A. Alsaedi, B. Ahmad, Synchronization between neurons coupled by memristor, Chaos, Solitons & Fractals 104 (2017) 435–442.
15. J. Ma, L. Mi, P. Zhou, Y. Xu, T. Hayat, Phase synchronization between two neurons induced by coupling of electromagnetic field, Appl. Math. Comput. 307 (2017) 321–328.
16. J. Ma, F. Wu, C. Wang, Synchronization behaviors of coupled neurons under electromagnetic radiation, Int. J. Mod. Phys. B 31 (2) (2017) 1650251.
17. F. Parastesh, H. Azarnoush, S. Jafari, B. Hatef, M. Perc, R. Repnik, Synchronizability of two neurons with switching in the coupling, Appl. Math. Comput. 350 (2019) 217–223.
18. S. Rakshit, B. K. Bera, D. Ghosh, S. Sinha, Emergence of synchronization and regularity in firing patterns in time-varying neural hypernetworks, Phys. Rev. E 97 (5) (2018) 052304.
19. M. Shafiei, F. Parastesh, M. Jalili, S. Jafari, M. Perc, M. Slavinec, Effects of partial time delays on synchronization patterns in izhikevich neuronal networks, Eur. Phys. J. B 92 (2) (2019) 36.
20. Y. Xu, Y. Jia, J. Ma, A. Alsaedi, B. Ahmad, Synchronization between neurons coupled by memristor, Chaos, Solitons & Fractals 104 (2017) 435–442.
21. X. Zhang, X. Lv, X. Li, Sampled-data-based lag synchronization of chaotic delayed neural networks with impulsive control, Nonlinear Dynam. 90 (3) (2017) 2199–2207.
22. H. Wang, Q. Wang, Q. Lu, Y. Zheng, Equilibrium analysis and phase synchronization of two coupled hr neurons with gap junction, Cogn. Neurodynam. 7 (2) (2013) 121–131.
23. S. Rakshit, B. K. Bera, M. Perc, D. Ghosh, Basin stability for chimera states, Sci. Rep. 7 (1) (2017) 2412.
24. C. Wang, J. Ma, A review and guidance for pattern selection in spatiotemporal system, Int. J Mod. Phys. B 32 (06) (2018) 1830003.
25. B. K. Bera, S. Majhi, D. Ghosh, M. Perc, Chimera states: Effects of different coupling topologies, EPL (Europhys. Lett.) 118 (1) (2017) 10001.
26. D. Dudkowski, Y. Maistrenko, T. Kapitaniak, Different types of chimera states: An interplay between spatial and dynamical chaos, Phys. Rev. E 90 (3) (2014) 032920.
27. Z. Faghani, Z. Arab, F. Parastesh, S. Jafari, M. Perc, M. Slavinec, Effects of different initial conditions on the emergence of chimera states, Chaos, Solitons & Fractals 114 (2018) 306–311.
28. F. Parastesh, S. Jafari, H. Azarnoush, B. Hatef, A. Bountis, Imperfect chimeras in a ring of four-dimensional simplified lorenz systems, Chaos, Solitons & Fractals 110 (2018) 203–208.
29. S. Majhi, B. K. Bera, D. Ghosh, M. Perc, Chimera states in neuronal networks: a review, Phys. Life Rev.
30. I. Omelchenko, A. Provata, J. Hizanidis, E. Schöll, P. Hövel, Robustness of chimera states for coupled fitzhugh-nagumo oscillators, Phys. Rev. E 91 (2) (2015) 022917.
31. J. Tang, J. Zhang, J. Ma, J. Luo, Noise and delay sustained chimera state in small world neuronal network, Sci. China Technol. Sci. (2018) 1–7, doi: 10.1007/s11431–017–9282–x.
32. Z. Wei, F. Parastesh, H. Azarnoush, S. Jafari, D. Ghosh, M. Perc, M. Slavinec, Nonstationary chimeras in a neuronal network, EPL (Europhys. Lett.) 123 (4) (2018) 48003.
33. Z. Rostami, S. Jafari, Defects formation and spiral waves in a network of neurons in presence of electromagnetic induction, Cogn. Neurodynam. 12 (2) (2018) 235–254.
34. Z. Rostami, K. Rajagopal, A. J. M. Khalaf, S. Jafari, M. Perc, M. Slavinec, Wavefront-obstacle interactions and the initiation of reentry in excitable media, Physica A 509 (2018) 1162–1173.
35. Y. Deng, B. Y. Liu, T. Wu, Y. Y. Shangguan, J. Ma, J. Tang, Parametric wave induces straight drift of spiral waves in excitable medium, EPL (Europhys. Lett.) 119 (5) (2017) 58002.
36. Y. Deng, B. Y. Liu, T. Wu, Y. Y. Shangguan, J. Ma, J. Tang, Parametric wave induces straight drift of spiral waves in excitable medium, EPL (Europhys. Lett.) 119 (5) (2017) 58002.
37. A. Verkhratsky, Physiology and pathophysiology of the calcium store in the endoplasmic reticulum of neurons, Physiological Rev. 85 (1) (2005) 201–279.
38. A. B. Parekh, J. W. Putney Jr, Store-operated calcium channels, Physiological Rev. 85 (2) (2005) 757–810.
39. R. Vepa, Modelling and estimation of chaotic biological neurons, IFAC Proceedings Volumes 42 (7) (2009) 27–32.
40. T. A. Giresse, K. T. Crepin, T. Martin, Generalized synchronization of the extended hindmarsh–rose neuronal model with fractional order derivative, Chaos, Solitons & Fractals 118 (2019) 311–319.